

# Self-assembly of actin monomers into long filaments: Brownian dynamics simulations

Kunkun Guo,<sup>1,a)</sup> Julian Shillcock,<sup>1,2</sup> and Reinhard Lipowsky<sup>1,b)</sup>

<sup>1</sup>Theory and Bio-Systems, Max Planck Institute of Colloids and Interfaces, 14424 Potsdam, Germany

<sup>2</sup>MEMPHYS-Centre for Biomembrane Physics, University of Southern Denmark, Campusvej 55, 5230 Odense M, Denmark

(Received 29 January 2009; accepted 4 June 2009; published online 1 July 2009)

Brownian dynamics simulations are used to study the dynamical process of self-assembly of actin monomers into long filaments containing up to 1000 actin protomers. In order to overcome the large separation of time scales between the diffusive motion of the free monomers and the relatively slow attachment and detachment processes at the two ends of the filaments, we introduce a novel rescaling procedure by which we speed all dynamical processes related to actin polymerization and depolymerization up by the same factor. In general, the actin protomers within a filament can attain three different states corresponding to a bound adenosine triphosphate (ATP), adenosine diphosphate with inorganic phosphate (ADP/P), and ADP molecule. The simplest situation that has been studied experimentally is provided by the polymerization of ADP-actin, for which all protomers are identical. This case is used to unravel certain relations between the filament's physical properties and the model parameters such as the attachment rate constant and the size of the capture zone, the detachment rate and the probability of the detached event, as well as the growth rate and waiting times between two successive attachment/detachment events. When a single filament is allowed to grow in a bath of constant concentration of free ADP-actin monomers, its growth rate increases linearly with the free monomer concentration in quantitative agreement with *in vitro* experiments. The results also show that the waiting time is governed by exponential distributions and that the two ends of a filament undergo biased random walks. The filament length fluctuations are described by a length diffusion constant that is found to attain a constant value at low ADP-actin concentration and to increase linearly with this concentration. It is straightforward to apply our simulation code to more complex processes such as polymerization of ATP-actin coupled to ATP hydrolysis, force generation by filaments, formation of filament bundles, and filament-membrane interactions. © 2009 American Institute of Physics. [DOI: 10.1063/1.3159003]

## I. INTRODUCTION

Actin filaments are major components of the cytoskeleton in eukaryotic cells and are usually several microns in length with a persistence length of the same order of magnitude.<sup>1</sup> Actin filaments are composed of many identical subunits of monomeric actin, a 43 kD globular protein with a few nanometers in diameter.<sup>1</sup> Actin filaments, which are arranged in an effectively two-stranded helical manner, have structural polarity. In the presence of adenosine triphosphate (ATP), the two ends of the filament also differ in their chemical composition; the filaments are then no longer in chemical equilibrium, but at steady state in a so-called “treadmilling” process with one end growing and the other end shrinking.<sup>2</sup> The growing end is known as the barbed or plus end of the filament whereas the shrinking end is called the pointed or minus end. Because of these dynamic properties, actin filaments play vital roles in many biological processes including

the organization of cell structures, transport of organelles and vesicles, cell division, cell motility, reproduction, and endocytosis.<sup>1-4</sup>

A full understanding of actin dynamics in cells requires to study the role of ATP hydrolysis in actin, but actin filaments can still assemble in the absence of ATP.<sup>5-9</sup> ATP-actin monomers can be hydrolyzed to ADP/P-actin (adenosine diphosphate with inorganic phosphate P bound noncovalently in the  $\gamma$ -phosphate position) and subsequently the inorganic phosphate P can be released, which leads to bound ADP-actin monomers. The three monomeric species, ATP-actin, ADP/P-actin, and ADP-actin, exhibit different attachment and detachment rates, which indicate that they assume different molecular conformations.<sup>9,10</sup> Indeed, each species has its own attachment and detachment rates, and thus its own equilibrium constants (critical concentrations) for the reactions at both the fast growing barbed end and the slow growing pointed end.<sup>11,12</sup> In addition, several possible mechanisms of ATP-actin hydrolysis in the filament have been proposed.<sup>8,13-16</sup> The first mechanism is “random hydrolysis,” in which any ATP-actin monomer can hydrolyze in a stochastic manner independent of the states of the adjacent monomers.<sup>13,14</sup> The hydrolysis rate is proportional to the

<sup>a)</sup>Electronic mail: guo@mpikg.mpg.de. Present address: College of Materials Science and Engineering, Huan University, Changsha 410082, People's Republic of China.

<sup>b)</sup>Electronic mail: lipowsky@mpikg.mpg.de.

amount of nontransformed nucleotide in the filament. The second mechanism is “vectorial hydrolysis” for which ATP hydrolysis occurs only at the interface between the ATP-actin cap and the remaining filament segment consisting of ADP-actin.<sup>15,16</sup>

Both computer simulations and analytic calculations have been used to study the complex self-assembly process of monomeric actin. Brownian dynamics (BD) simulations have been applied to determine the thermodynamics and kinetics of actin nucleation and explore the attachment of actin monomers to tetramers.<sup>17</sup> Monte Carlo simulations and analytic calculations<sup>13,16</sup> have also been utilized to study the growth dynamics at one end of a single actin filament, taking the hydrolysis of ATP-actin monomers into account, and these theoretical studies exhibit the large filament length fluctuations observed in recent experiments.<sup>18</sup> However, so far these simulation studies have not addressed filament growth governed by diffusive motion of actin monomers in bulk solvent and the associated dynamical processes of self-assembly, which lead to filaments that can contain thousands of protomers and have structural polarity at the two ends.

In this article, we will study the self-assembly or polymerization of relatively long filaments using BD.<sup>19,20</sup> In order to do so, we will introduce a coarse-grained model, in which we ignore the atomic details of the actin monomers and describe their interactions by soft-core potentials as widely used in dissipative particle dynamics. In this way, we reduce the number of degrees of freedom and are able to use a larger time step for the integration of the equations of motion.

In order to overcome the large separation of time scales between the diffusive motion of the free monomers and the relatively slow attachment and detachment processes at the two ends of the filaments, we introduce an overall rescaling factor, denoted by  $b$ , for all attachment and detachment rates. In this way, we will speed up all dynamical processes related to actin polymerization and depolymerization by the same factor  $b$ . As a result, the real filament at time  $t$  will correspond to the simulated filament at time  $\hat{t}=t/b$ . Our rescaling procedure also involves the rescaling of the actin monomer concentration, which allows us to keep the spatial resolution of our simulations comparable to the size of a single actin monomer.

To demonstrate that our approach can be used to simulate rather long filaments, we focus on the simplest situation, which is provided by the self-assembly of ADP-actin as studied experimentally in Refs. 5–9. This case is used to unravel certain relations between the filaments’ physical properties and the model parameters such as the relation between the attachment rate constant and the size of the capture zone between the detachment rate and the probability of the detached event, as well as between the growth rate and the waiting times between two successive attachment/detachment events. When a single filament is allowed to grow in a bath of constant concentration of free ADP-actin monomers, its growth rate increases linearly with the free monomer concentration in quantitative agreement with *in vitro* experiments. In addition, we also analyze the fluctua-

tions in the length of the polymerizing and depolymerizing filaments.

This article is organized as follows. Section II contains a detailed description of our method, including the algorithm for the attachment/detachment events and the rescaling procedure. In Sec. III, we present the results for the self-assembly or polymerization of ADP-actin monomers for which all actin protomers remain in the ADP state. In this latter section, we describe the various relations between the model parameters and the filaments’ physical properties. Finally, a brief summary and outlook is given in Sec. IV.

## II. THEORETICAL DESCRIPTION

In the following, we use BD simulations to study the assembly of freely diffusing actin monomers into a single filament that grows to several microns in length. The monomers represent the 43-kDa globular form of actin, and they attach and detach from the two ends of the filament via a stochastic process whose parameters are determined by comparing the simulation results with experimental data. The theory of Brownian motion was developed to describe the dynamic behavior of particles whose mass and size are much larger than those of the host medium particles.<sup>19,20</sup> Thus, it is ideally suited for the study of actin monomers in aqueous solution and is useful for many biological systems *in vivo* or *in vitro*.

Here, we briefly describe the equations of motion used in classical BD simulation and the most commonly used algorithm proposed by Ermak and McCammon.<sup>20</sup> In this algorithm, if  $\mathbf{r}_i(t)$  is the position vector of the center of mass of the  $i$ th particle at the previous time step  $t$ , then the position vector  $\mathbf{r}_i(t+\Delta t)$  is given by

$$\mathbf{r}_i(t+\Delta t) = \mathbf{r}_i(t) + \frac{\Delta t}{k_B T} \sum_j D_{ij} \cdot \mathbf{F}_{ij} + \mathbf{R}_i(\Delta t), \quad (1)$$

where  $k_B$  is the Boltzmann constant,  $T$  is the temperature, and  $\mathbf{F}_{ij}$  is the force exerted on particle  $i$  by particle  $j$ . In the absence of hydrodynamic interactions mediated by the fluid, the diffusion tensor  $D_{ij}$  is diagonal, isotropic, and constant and is given by

$$D_{ij} = D \delta_{ij} = \frac{k_B T}{6\pi\eta r_{pa}} \delta_{ij}, \quad (2)$$

with the diffusion constant  $D$ , the solvent viscosity  $\eta$ , and the particle radius  $r_{pa}$ . The components of the vector  $\mathbf{R}_i(\Delta t)$  are random displacements that arise from the collisions of particle  $i$  with the solvent particles that are not considered explicitly. The displacement vector  $\mathbf{R}_i(\Delta t)$  is taken to be a Gaussian random variable whose average value vanishes,  $\langle \mathbf{R}_i(\Delta t) \rangle = 0$ , and whose variance is given by  $\langle \mathbf{R}_i(\Delta t) \cdot \mathbf{R}_j(\Delta t) \rangle = 6D_{ij}\Delta t$ .

In our coarse-grained model, actin monomers are constructed out of particles subject to configuration-dependent forces that effectively represent the complex forces between real actin monomers. We do not include electrostatic interactions explicitly, assuming that they are screened between free monomers, but incorporate their effects on monomer-filament interactions via the capture zone for monomer

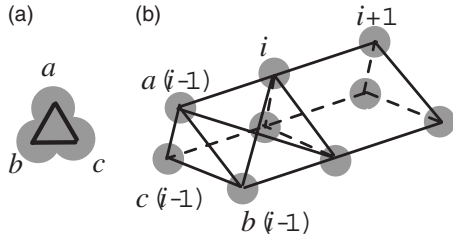


FIG. 1. Coarse-grained model of monomer and filament (a) actin monomer built up from three particles labeled by  $a$ ,  $b$ , and  $c$  and connected into an equilateral triangle. (b) These triangles are tied together into a filament by Hookean springs, which are between adjacent  $a$ , adjacent  $b$ , and adjacent  $c$  particles as well as between all next-nearest neighbors particles within the filament (for clarity, only two next-nearest neighbor bonds are shown).

attachment,<sup>17,21</sup> see Sec. II A. Within a filament, monomers are bound together using both spring and bending potentials, which together make the filament stiff and prevent it from breaking apart. Because the interactions between free monomers are not relevant to the filament's growth, we use soft-core potentials between free monomers rather than hard-core potentials such as Lennard-Jones potentials. The nonbonded force between two particles  $i$  and  $j$  with their center of mass separated by a distance  $r_{ij}=|\mathbf{r}_{ij}|=|\mathbf{r}_i-\mathbf{r}_j|$  has the same form as in dissipative particle dynamics<sup>22</sup> and is given by

$$\mathbf{F}_{ij} = \begin{cases} a_{ij}(1 - r_{ij}/r_0)\hat{\mathbf{r}}_{ij} & \text{for } r_{ij} < r_0 \\ 0 & \text{for } r_{ij} \geq r_0. \end{cases} \quad (3)$$

The range of the force is set by the length scale  $r_0$ , the parameter  $a_{ij}$  is the maximum repulsion between particles of type  $i$  and  $j$ , and the unit vector  $\hat{\mathbf{r}}_{ij}=\mathbf{r}_{ij}/|\mathbf{r}_{ij}|$  points from particle  $j$  to particle  $i$ . The force is always finite and is repulsive for positive  $a_{ij}$ . This force law is computationally cheap and keeps free monomers apart unless one studies very high monomer concentrations. In the simulation,  $a_{ij}$  is equal to 25 in units of  $k_B T/r_0$ .

Each actin monomer is composed of three spherical particles of diameter  $r_0=2r_{pa}$  connected into an equilateral triangle by harmonic bonds. The particles are labeled as  $a$ ,  $b$ , and  $c$ , as shown in Fig. 1(a). The harmonic bond potential is expressed as

$$U_2 = \frac{1}{2}k_2(|\mathbf{r}| - l_1)^2, \quad (4)$$

where  $|\mathbf{r}|$  represents the distance between adjacent particles in the actin monomer. The spring constant  $k_2$  and the unstretched length  $l_1$  are chosen so as to fix the average bond length to the desired value as given by  $0.75r_0$ . This choice ensures that the fluctuations in the monomer's shape and diameter are small compared to their mean values. A three-body potential

$$U_3(a, b, c) = k_3[1 - \cos(\phi - \phi_1)] \quad (5)$$

depending on the bending stiffness  $k_3$  is used to constrain the angle between the adjacent particles, where  $\phi$  is the angle between two bonds connecting the three particles  $a$ ,  $b$ , and  $c$ , and  $\phi_1$  is the desired average value of  $\phi$ , which is taken to be  $\phi_1 = \pi/3$ .

Actin monomers attach to the ends of a growing filament according to the mechanism described in Sec. II A. Once

bound, they are held in place using Hookean springs, as illustrated in Fig. 1(b). The desired bond length  $l_2$  between the  $i-1$ th and the  $i$ th monomer labeled by  $a$ ,  $b$ , and  $c$  is  $l_2 = 0.5r_0$ , whereas the desired bond length  $l_3$  between  $a(i-1)$  and  $b(i)$  is  $l_3 = 0.86r_0$ . The harmonic bond potentials are given by

$$U'_2(a(i-1), a(i)) = \frac{1}{2}k_2(|\mathbf{r}_{a(i-1), a(i)}| - l_2)^2 \quad (6)$$

and

$$U''_2(a(i-1), b(i)) = \frac{1}{2}k_2(|\mathbf{r}_{a(i-1), b(i)}| - l_3)^2. \quad (7)$$

Additional three-body potentials of the form

$$U'_3(a(i-1), a(i), a(i+1)) = k_3[1 - \cos(\phi - \phi_2)] \quad (8)$$

are acting along the filament between the bonds connecting three adjacent monomers in the filament, and  $\phi$  is the angle which has the desired average value  $\phi_2 = \pi$  corresponding to a straight filament. As in Eqs. (6)–(8), potentials  $U'_2$ ,  $U''_2$ , and  $U'_3$  are present between the  $b(i)$  and  $c(i)$  particles, see Fig. 1. We take  $k_2 = 128k_B T/r_0^2$  and  $k_3 = 10k_B T$ . The architecture shown in Fig. 1 and the corresponding force parameters are chosen in order to obtain a sufficiently rigid filament.

In order to confine the shape fluctuations of a single filament, the assembled filament is embedded in a cylindrically symmetric potential oriented along the filament's axis, i.e., the long axis of the simulation box. This harmonic potential  $U_4$  has the form

$$U_4(i) = \frac{1}{2}k_4(|\mathbf{r}_{i,m}|)^2 \quad (9)$$

with spring constant  $k_4 = 20k_B T/r_0^2$ , where  $|\mathbf{r}_{i,m}|$  is the distance of each particle of the  $i$ th monomer in the filament projected along the long axis of the simulated box. It is important to note that this force is only applied to monomers that are already bound to the filament: it does not apply to free monomers or to a monomer in the process of attaching to a filament's end.

## A. Algorithm for monomer attachment and detachment

Actin filament growth proceeds in several stages, the first of which requires three monomers to bind simultaneously in order to seed the growing filament.<sup>23</sup> Because we are interested in the dynamics of long filaments, we do not include this initial nucleation process in our model. Instead, a single filament is seeded at the beginning of the simulation with two monomers that are labeled as its barbed and pointed ends, respectively, and its subsequent growth is a stochastic process as free actin monomers diffuse to the ends of the filament and attach, or the terminal monomers detach. The filament length only changes by the addition or loss of monomers at its ends; no filament breakage is allowed. The effective binding and unbinding rates at the filament's two ends are controlled by independent parameters, and once the filament has a length in excess of a hundred monomers or so, the two ends are observed to grow in an uncorrelated manner.

The binding of a free actin monomer to a growing filament is a complex process that we reduce to several steps. A

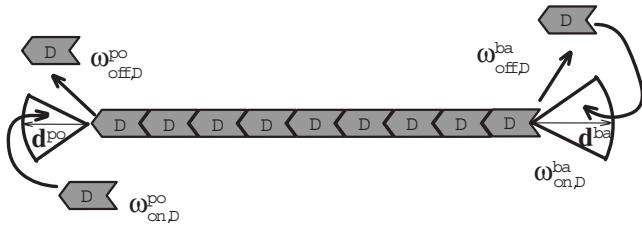


FIG. 2. Schematic illustration of the computational mechanism of ADP-filament growth by attachment and detachment of monomers to its ends. Single actin monomers with a bound ADP molecule are labeled with the letter “D.” The conical regions at the filament’s ends are capture zones with independent radius  $d^{ba}$  and  $d^{po}$  at the filament’s barbed and pointed ends, whose sizes control the rate of free monomer attachment events. Detachment of the terminal monomers at the filament’s barbed and pointed ends is controlled by two more independent parameters,  $\omega_{\text{off},D}^{ba}$  and  $\omega_{\text{off},D}^{po}$ . Note that the rates of monomer attachment to the filament ends,  $\omega_{\text{on},D}^{ba}$  and  $\omega_{\text{on},D}^{po}$ , are not parameters of the model but are determined by the capture zone size and the free monomer concentration.

free actin monomer binds to one end of the filament if it approaches this end within a certain distance in an appropriate orientation. At each end of the filament, a conical *capture zone* is defined with its apex located at the terminal monomer and a spherical cap for its base. The zone is cut from a sphere, and its radius is represented by  $d^{ba}$  and  $d^{po}$  for barbed and pointed ends, respectively, and its internal angle is  $60^\circ$ , as shown in Fig. 2. The distance  $d$  is chosen independently for the barbed and pointed ends of the filament, but its radius is chosen to be between  $0.8r_0$  and  $4r_0$ , i.e., approximately the diameter of an actin monomer in the simulation. The conical shape of the capture zone represents the lumped effects of electrostatic and van der Waals interactions in guiding a monomer onto the filament’s end.<sup>21</sup> These effects are found to be different at the barbed and pointed ends, and the attachment rate constant for ADP-actin monomers is about 21-fold larger for the barbed end than for the pointed end, see Table I. The filament therefore has a fast-growing barbed end and a slow-growing pointed end. Varying the parameter  $d$  provides the possibility of tuning the attachment rates at either end in such a way that they match the rate constants observed in the experiment.

Actin monomers usually contain a bound nucleotide that can attain different internal states. We attach a flag to each monomer that can take a number of values corresponding to the internal state of the bound nucleotide: ATP, ADP/P, or ADP.<sup>9,14</sup> ATP cleavage transforms ATP-actin into ADP/P-actin while P release changes ADP/P-actin into ADP-actin. Each of these monomeric species can bind to and unbind from both ends with different rates as observed in the experiment. The parameters of the model are then chosen to de-

TABLE I. Attachment rate constants  $\kappa_{\text{on}}$ , detachment rates  $\omega_{\text{off}}$ , and equilibrium (or critical) concentration  $C_{D,\text{eq}}$  for Mg-ADP-actin (Ref. 12) at barbed and pointed ends of actin filaments.

$\kappa_{\text{on},D}^{ba}, \mu\text{M}^{-1} \text{s}^{-1}$	$2.9 \pm 0.21$
$\kappa_{\text{on},D}^{po}, \mu\text{M}^{-1} \text{s}^{-1}$	$0.134 \pm 0.03$
$\omega_{\text{off},D}^{ba}, \text{s}^{-1}$	$5.4 \pm 0.14$
$\omega_{\text{off},D}^{po}, \text{s}^{-1}$	$0.25 \pm 0.04$
$C_{D,\text{eq}}, \mu\text{M}$	$1.8 \pm 0.14$

pend on these flags. The detachment rates for the terminal monomers to leave the filament,  $\omega_{\text{off}}^{ba}$  and  $\omega_{\text{off}}^{po}$ , have concomitant independent values that depend on their nucleotide states. The ADP monomers can detach from the barbed and pointed ends with a dwell time  $\tau_D$  that is smaller than the time interval  $\Delta t$ , and the corresponding probabilities<sup>24</sup> for detachment are given by

$$\text{Prob}(\tau_D^{ba} < \Delta t) = 1 - \exp[-\omega_{\text{off},D}^{ba}\Delta t] \quad (10)$$

and

$$\text{Prob}(\tau_D^{po} < \Delta t) = 1 - \exp[-\omega_{\text{off},D}^{po}\Delta t], \quad (11)$$

respectively. The detachment events at both ends of the filament are taken to be uncorrelated.

To summarize, once the actin monomers have been constructed out of the basic particles and the binding potentials between particles in the monomers and between monomers in a filament have been specified, our model of filament growth contains the following parameters: (i) the concentration of free actin monomers in the bulk and their bulk diffusion coefficient, (ii) the size and angle of capture zones, which determine the mean attachment rate constant of monomers to the filament and are assumed to be independent of the monomer’s internal states, (iii) the rates of the terminal monomers detaching from the filament ends, which depend, in general, on the monomeric species, (iv) the number  $q$  assigned to the different species, which is  $q=1$  for ADP-actin,  $q=2$  when two species are distinguished, and  $q=3$  for the complete model in which the monomer may contain a bound ATP, ADP/P, or ADP, and (v) the transition rates that govern the transition from one monomeric species to another. We note here that whereas our model contains explicit parameters for the detachment of monomers from a filament, the attachment rate constant must be measured from the simulations as we only specify the sizes and shapes of the capture zones, which combine with the random diffusion of the bulk monomers to yield the actual monomer binding rates.

The simplest case is to allow only a single bound nucleotide state, namely, ADP, i.e., to ignore the hydrolysis of bound ATP-actin. The filament’s dynamics then reduces to that of a biased one-dimensional random walk. Increasing the complexity of the model by allowing the monomers to possess two or three internal states is straightforward and will be described in subsequent publications.

## B. Simulation parameters

ADP-actin monomers at a chosen concentration  $C_D$  are randomly distributed throughout the cuboidal simulation box of constant volume  $V=L_xL_yL_z$ , where  $L_x=30$ ,  $L_y=30$ , and  $L_z=400$  are the three box dimensions in units of the coarse-grained particle diameter  $r_0$ . A single filament is seeded with two monomers and subsequently allowed to grow by the addition of new monomers to its ends. The width of an actin filament is usually measured as  $7 \text{ nm}$ ,<sup>1</sup> which is close to  $3r_0/2$  according to the coarse-grained model for an actin monomer in Fig. 1. The length scale  $r_0$  in the simulations is then close to  $5 \text{ nm}$ . Periodic boundary conditions are used in

all three dimensions to minimize edge effects. The simulation box is long in the  $Z$  direction so that the filament can grow without being affected by the periodic boundary of this axis. The  $X$  and  $Y$  dimensions are smaller but still chosen large enough that the filament dynamics is independent of the box size.

As the polymerization/depolymerization reaction proceeds, the total number of free actin monomers in the bulk is kept constant so that the growth occurs under conditions of constant free monomer concentration. This is achieved by adding a randomly chosen monomer distant from the filament at the instant that a monomer binds to the filament and removing the newly detached monomer to avoid its immediate reattaching. The latter procedure is justified by the separation of time scales between diffusive steps in the bulk and attachment and detachment events at the two filament ends.<sup>25</sup> A typical run is carried out for  $10^8$  steps or until the length of a filament grows to the size of the simulation box or shrinks to zero. The basic time scale  $t_{sc}$  of the simulations is extracted from the bulk diffusion constant  $D$  of free actin monomers, as defined in Eq. (2). A typical experimental value for this constant is about  $10^{-11} \text{ m}^2 \text{ s}^{-1}$  *in vivo*.<sup>26</sup> In the simulations, we find that the diffusion constant of a monomer containing three particles is one-third of the single particle diffusion constant. Hence, we set the diffusion constant of a single particle equal to  $D=3 \times 10^{-11} \text{ m}^2 \text{ s}^{-1}$ . The diffusion constant of a particle within a monomer is calculated from

$$D = \lim_{t \rightarrow \infty} \frac{1}{N} \sum_{i=1}^N \langle [\mathbf{r}_i(t) - \mathbf{r}_i(0)]^2 \rangle / 6Nt, \quad (12)$$

where  $N$  is the number of particles in the simulation and is three times the number of actin monomers, see Fig. 1. We now define the dimensionless diffusion constant  $D' \equiv t_{sc} D / r_0^2$  for a single particle with the length scale  $r_0 = 5 \text{ nm}$ . In the simulations, this dimensionless diffusion constant  $D'$  is equal to one which implies the basic time scale  $t_{sc} = r_0^2 / D = 0.83 \text{ } \mu\text{s}$ . Furthermore, the time step  $\Delta t$  in the BD [Eq. (1)] is chosen to be  $\Delta t = 0.001 t_{sc} = 0.8 \text{ ns}$ .

Random initial configurations are created by assigning random position coordinates to all particles, subject to the constraint that particles in a monomer are within a bond length of each other. In order to compare the results from distinct simulations above or below the critical concentrations, the same length of a filament is generated before starting to analyze the results. A filament with a specified length is obtained simply by letting it grow using the attachment algorithm mentioned above, and then setting the capture zone size and unbinding constants to the chosen values. Subsequently, the filament continues to polymerize and depolymerize at rates determined by the chosen parameters.

### C. Time scales involved in actin polymerization and depolymerization

Any particle-based simulation study of actin polymerization and depolymerization encounters a fundamental difficulty, which is related to the large separation of time scales between the diffusive motion of free actin monomers in the bulk and the typical attachment and detachment times at the

two filament ends. As mentioned in Sec. II B, the bulk diffusion coefficient for free actin monomers is about  $10^{-7} \text{ cm}^2 \text{ s}^{-1}$ . This implies that the diffusive time scale  $t_{sc}$  is taken to be  $0.8 \text{ } \mu\text{s}$ . The integration time step  $\Delta t$  is then given by  $\Delta t = 1 \times 10^{-3} t_{sc}$ .

The typical attachment and detachment times of the actin monomers are typically much larger than  $t_{sc}$ . In the following, we will focus on the ionic conditions discussed in Ref. 12 and the associated rate constants are listed in Table I. For these conditions, the detachment rate  $\omega_{off,D}^{ba}$  of a  $D$  monomer at the barbed end was estimated to be  $\omega_{off,D}^{ba} = 5.4 \text{ s}^{-1}$ . Thus, the average time between two detachment events is given by about 200 ms, which is much larger than the diffusive time scale  $t_{sc} = 0.8 \text{ } \mu\text{s}$ . Furthermore, the attachment rate of a  $D$  monomer at the barbed end has the general form  $\omega_{on,D}^{ba} = \kappa_{on,D}^{ba} C_D$  and, thus, increases linearly with the concentration of the  $D$  monomers. For the rate constants listed in Table I, the attachment rate constant  $\kappa_{on,D}^{ba}$  at the barbed end was estimated to be  $\kappa_{on,D}^{ba} = 2.9 \text{ } \mu\text{M}^{-1} \text{ s}^{-1}$ . If the barbed end is in equilibrium, one has  $\omega_{off,D}^{ba} = \kappa_{on,D}^{ba} C_{D,eq}^{ba}$ , which leads to the ‘‘critical’’ or equilibrium concentration  $C_{D,eq}^{ba} = 1.8 \text{ } \mu\text{M}$ . For  $C_D = C_{D,eq}^{ba}$ , the average time between two attachment events is also given by about 200 ms.

Therefore, if we simulated the system at a concentration that is comparable to the critical concentration of the barbed end and used the physical values of the detachment and attachment rates, the average time between detachment or attachment events would be of the order of  $200 \text{ ms} = 2.5 \times 10^5 t_{sc} = 2.5 \times 10^8 \Delta t$ . This implies that we would hardly see a single attachment or detachment event during  $10^8$  time integration steps. Obviously, such a scheme would be very inefficient in order to simulate the polymerization and depolymerization of actin filaments.

### D. Rescaling procedure

To improve the efficiency of our particle-based algorithm, we will speed up all attachment and detachment processes simultaneously by the same dimensionless factor  $b$ . In the simulations described below, we will use the value  $b = 1352$ . Thus, we multiply all detachment rates by  $b$  and define the rescaled rates

$$\hat{\omega}_{off,D}^{ba} \equiv b \omega_{off,D}^{ba} \quad \text{and} \quad \hat{\omega}_{off,D}^{po} \equiv b \omega_{off,D}^{po}. \quad (13)$$

Likewise, the rescaled attachment rates are defined by

$$\hat{\omega}_{on,D}^{ba} \equiv b \omega_{on,D}^{ba} \quad \text{and} \quad \hat{\omega}_{on,D}^{po} \equiv b \omega_{on,D}^{po}. \quad (14)$$

In the real system, the attachment rates are proportional to the actin concentration  $C_D$  and have the form

$$\omega_{on,D}^{ba} = \kappa_{on,D}^{ba} C_D \quad \text{and} \quad \omega_{on,D}^{po} = \kappa_{on,D}^{po} C_D, \quad (15)$$

which defines the ratio

$$\omega_{on,D}^{ba} / \omega_{on,D}^{po} = \kappa_{on,D}^{ba} / \kappa_{on,D}^{po} \equiv X_{\kappa}. \quad (16)$$

As the experimental parameters are listed in Table I, one has  $X_{\kappa} = 21.6$ . In the simulations, the attachment rate constants  $\hat{\kappa}_{on,D}$  are determined by the sizes,  $d^{ba}$  and  $d^{po}$ , of the two capture zones in front of the two filament ends. Thus, we will choose these capture zone sizes in such a way that

TABLE II. Rescaled attachment rate constants  $\hat{\kappa}_{\text{on}}$ , detachment rates  $\hat{\omega}_{\text{off}}$ , and equilibrium (or critical) concentration  $\hat{C}_{D,\text{eq}}$  as used in the simulations.

$\hat{\kappa}_{\text{on},D}^{\text{ba}}, \mu\text{M}^{-1} \text{s}^{-1}$	$79.31 \pm 2.28$
$\hat{\kappa}_{\text{on},D}^{\text{po}}, \mu\text{M}^{-1} \text{s}^{-1}$	$3.67 \pm 0.083$
$\hat{\omega}_{\text{off},D}^{\text{ba}}, \text{s}^{-1}$	$7.3 \times 10^3$
$\hat{\omega}_{\text{off},D}^{\text{po}}, \text{s}^{-1}$	$3.38 \times 10^2$
$\hat{C}_{D,\text{eq}}, \mu\text{M}$	$92.04 \pm 2.56$

$$\hat{\kappa}_{\text{on},D}^{\text{ba}}/\hat{\kappa}_{\text{on},D}^{\text{po}} = \kappa_{\text{on},D}^{\text{ba}}/\kappa_{\text{on},D}^{\text{po}} = X_{\kappa}. \quad (17)$$

In addition, we want to simulate the system with a spatial resolution of the order of the monomer size  $r_0$  and, thus, want to choose the capture zone sizes to be of the order of  $r_0$ . For  $X_{\kappa}=21.6$ , a convenient choice for the capture zone sizes is found to be  $d^{\text{ba}}=2.5r_0$  at the barbed end and  $d^{\text{po}}=0.8413r_0$  at the pointed end, see Sec. III and Appendix. For the chosen capture zone sizes, we determine the corresponding attachment rate constants  $\hat{\kappa}_{\text{on},D}$  by measuring the growth rate of the filaments and define the rescaling factor

$$b_{\kappa} \equiv \hat{\kappa}_{\text{on},D}^{\text{ba}}/\kappa_{\text{on},D}^{\text{ba}} = \hat{\kappa}_{\text{on},D}^{\text{po}}/\kappa_{\text{on},D}^{\text{po}}. \quad (18)$$

For the capture zone sizes  $d^{\text{ba}}=2.5r_0$  and  $d^{\text{po}}=0.8413r_0$ , we obtain  $b_{\kappa}=27.3$  according to the experimental parameters listed in Table I and the simulation results of Appendix given in Table II. It then follows from the two relations [Eqs. (18) and (14)] that the concentration  $C_D$  in the real system and the concentration  $\hat{C}_D$  used in the simulations are linearly related as

$$C_D \equiv (b_{\kappa}/b)\hat{C}_D \equiv \hat{C}_D/49.5. \quad (19)$$

### III. RESULTS

In the present study, we focus on the simplest system which contains only ADP-actin monomers. Such a system already leads to actin polymerization and filament growth, as shown experimentally, and provides a useful test for our simulation code. The filament's dynamics then reduces to that of a biased one-dimensional random walk, and its growth is now determined by the rates of ADP-actin monomers entering the capture zones at the filament ends and the detachment rates of the terminal monomers. The structural polarity of actin filaments at two ends is reflected in different attachment and detachment rates. The rates for reactions of Mg-actin at barbed ends and pointed ends of actin filaments have been summarized recently.<sup>12</sup> These rates show that ADP-actin monomers have different attachment and detachment rates but the same critical concentrations at the two ends of the filament. To match the experimental values,<sup>12</sup> we choose the simulation parameters that control the attachment of monomers at the barbed and pointed ends so that their ratio is similar to that observed in experiments, namely, that the attachment rate constant at the barbed end is  $X_{\kappa}=21.6$  times that at the pointed end, compared to Eq. (16). As mentioned, this requires that the radii of the capture zones are  $d^{\text{ba}}=2.5r_0$  and  $d^{\text{po}}=0.8413r_0$  for the barbed and pointed ends, respectively. As listed in Table II, the ratio of the detachment rates is set close to the experimentally determined value of

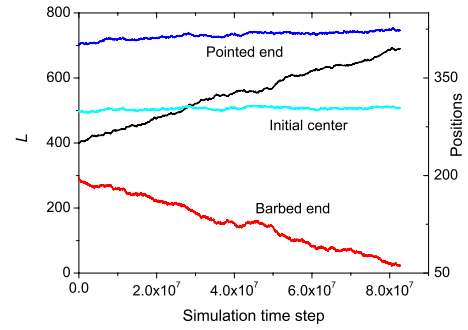


FIG. 3. Time evolution of actin protomer number  $L(\hat{t})$  (black solid line, left Y axis); positions (right Y axis) of barbed end (red solid line), pointed end (blue solid line), and the initial center (cyan solid line) in the filament vs simulation time step. The capture zone sizes are  $d^{\text{ba}}=2.5r_0$  and  $d^{\text{po}}=0.8413r_0$  and the detachment rates are  $\hat{\omega}_{\text{off},D}^{\text{ba}}=7.3 \times 10^3 \text{ s}^{-1}$  and  $\hat{\omega}_{\text{off},D}^{\text{po}}=338 \text{ s}^{-1}$  at the barbed and pointed ends, respectively.

21.6 by choosing  $\hat{\omega}_{\text{off},D}^{\text{ba}}=7.3 \times 10^3 \text{ s}^{-1}$  and  $\hat{\omega}_{\text{off},D}^{\text{po}}=338 \text{ s}^{-1}$ , and their absolute values are a factor of  $b=1352$  times larger than the experimental values, so as to rapidly attain the steady-state growth behavior of the filament, thereby reducing the computational cost.

A filament is allowed to assemble in the simulation box until it contains  $\sim 400$  monomers and measurements of its properties are subsequently collected. We recall that the free monomer concentration  $C_D$  in the simulation box is held constant during the filament growth. Figure 3 shows the time evolution of the number of actin protomers, the positions of the barbed and pointed ends of the filament, and the position of the center of mass of the preassembled filament, which we call the initial center. A linear increase in the number of actin protomers as a function of simulation time is observed in Fig. 3 as well as linear changes in the positions of the barbed and pointed ends. By contrast, the initial center moves back and forth with small fluctuations, indicating that the filament is not displaced and does not exhibit treadmilling.

#### A. Definition of growth rate

The time-dependent filament length  $L=L(t)$  will be measured in units of the monomer size and is, thus, equal to the total number of protomers incorporated into the filament at time  $t$ . The excess number of protomers that has been added to the barbed and pointed ends after time  $t$  will be denoted by  $n^{\text{ba}}=n^{\text{ba}}(t)$  and  $n^{\text{po}}=n^{\text{po}}(t)$ , respectively. Thus, we have the relation

$$L(t) = L_0 + n(t) \quad \text{with} \quad n \equiv n^{\text{ba}} + n^{\text{po}}, \quad (20)$$

where  $L_0$  is the initial filament length at time  $t=0$ . The average growth rates for the two ends of the filament are then given by

$$\frac{d\langle n^{\text{ba}} \rangle}{dt} = \kappa_{\text{on},D}^{\text{ba}} C_D - \omega_{\text{off},D}^{\text{ba}} \quad (21)$$

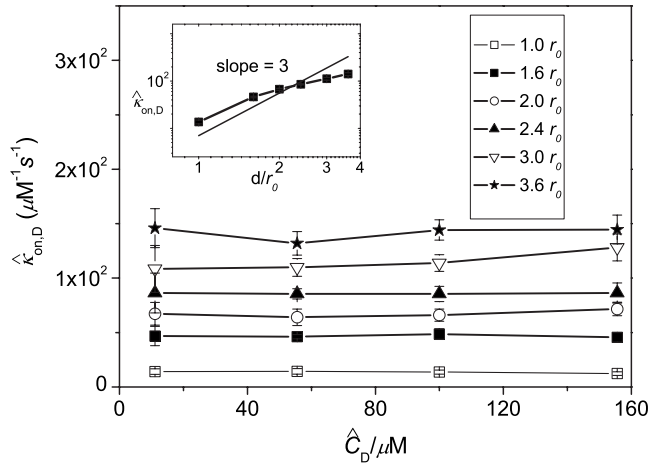


FIG. 4. Dependence of kinetic rate constants  $\hat{\kappa}_{on,D}$  on monomer concentration  $\hat{C}_D$  for different values of the capture zone size  $d$ , which is varied from  $d=1.0r_0$  (open squares) to  $d=3.6r_0$  (closed stars). In the inset, the mean kinetic rate constants at each capture zone are plotted logarithmically as a function of height  $d/r_0$ ; the straight line has slope 3. In these simulations, we chose  $\hat{\omega}_{off,D}=0$ .

and

$$\frac{d\langle n^{po} \rangle}{dt} = \kappa_{on,D}^{po} C_D - \omega_{off,D}^{po}, \quad (22)$$

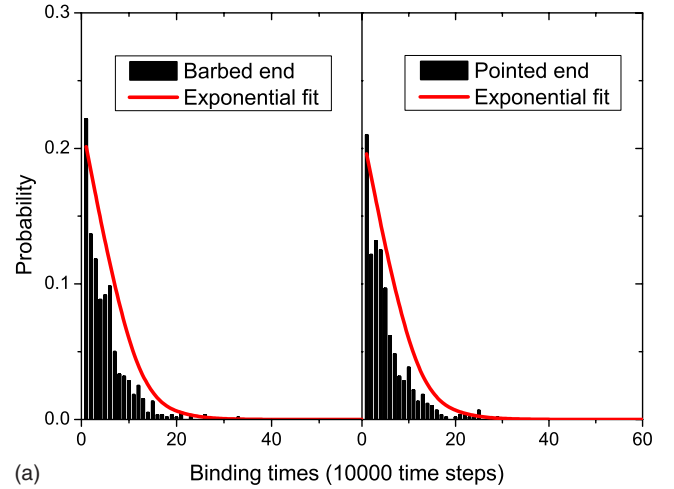
where  $\kappa_{on,D}^{ba}$  and  $\kappa_{on,D}^{po}$  are the two attachment rate constants for  $D$  monomers. Combining these expressions, the growth rate of the filament  $J_g(C_D)$  defined as the time derivative of the average number  $\langle L \rangle$  of actin protomers satisfies the relation

$$J_g(C_D) = \frac{d\langle L \rangle}{dt} = \frac{d\langle n^{ba} + n^{po} \rangle}{dt} = (\kappa_{on,D}^{ba} + \kappa_{on,D}^{po}) C_D - (\omega_{off,D}^{ba} + \omega_{off,D}^{po}). \quad (23)$$

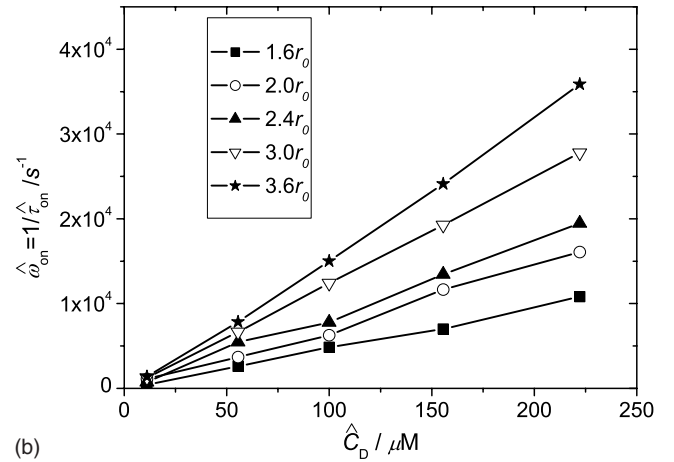
If we now introduce the rescaled growth rate  $\hat{J}_g \equiv bJ_g$  and the rescaled time  $\hat{t} \equiv t/b$ , we obtain the evolution equation

$$\hat{J}_g(\hat{C}_D) = \frac{d\langle L \rangle}{d\hat{t}} = \frac{d\langle n^{ba} + n^{po} \rangle}{d\hat{t}} = (\hat{\kappa}_{on,D}^{ba} + \hat{\kappa}_{on,D}^{po}) \hat{C}_D - (\hat{\omega}_{off,D}^{ba} + \hat{\omega}_{off,D}^{po}). \quad (24)$$

Since the average growth rate of the barbed end is larger than that of the pointed end, the positions of the barbed and pointed ends are nonsymmetric with respect to the initial center. The barbed end deviates rapidly from the initial center, whereas the initial center itself performs random fluctuations about its initial position, which is in accordance with the results shown in Fig. 3. In addition, since the right hand in Eq. (24) is constant for constant monomer concentration, the total actin protomer number  $L(\hat{t})$  should linearly increase or decrease as a function of time, depending on whether the free monomer concentration  $\hat{C}_D$  exceeds or is below the critical concentration,  $\hat{C}_{D,eq} = \hat{\omega}_{off,D}^{po} / \hat{\kappa}_{on,D}^{po} = \hat{\omega}_{off,D}^{ba} / \hat{\kappa}_{on,D}^{ba}$ , which is close to  $93.2 \mu\text{M}$  in the simulation, see Fig. 6.



(a) Normalized histograms for time intervals between successive monomer attachments at barbed and pointed ends. The width of the bins is 10 000 time steps, the probability of attachment is approximately exponentially distributed,  $d^{ba}=d^{po}=3.0r_0$ .



(b) The inverse mean waiting time  $\hat{\omega}_{on}^{-1}$ , which is equal to the attachment rate as a function of monomer concentration at different capture zone sizes.

## B. Attachment rate constants

Figure 4 presents the dependence of the attachment rate constants  $\hat{\kappa}_{on,D}$  on monomer concentration  $\hat{C}_D$  for different capture zone sizes and  $\hat{\omega}_{off,D}=0$ . Small variations in the attachment rate constant are seen for different monomer concentrations at a given capture zone size, but the mean value is almost independent of the concentration. Thus, we conclude that the attachment rate constants are essentially independent of monomer concentration for a given capture zone. In addition, a small increase in the size of the capture zone leads to a large increase in the attachment rate constant. To further understand the dependence of attachment rate constants on capture zone sizes, the mean attachment rate constants are presented in the inset of Fig. 4 for each capture zone. Inspection of this figure shows that the mean attachment rate constant increases approximately as  $(d/r_0)^3$ , i.e., with the third power of the capture zone size  $d$ . In the simulations, the capture zone has the shape of a spherical cone cut out from a sphere of radius  $d$  and its volume is proportional to  $d^3$ . The attachment rate constant is theoretically related to

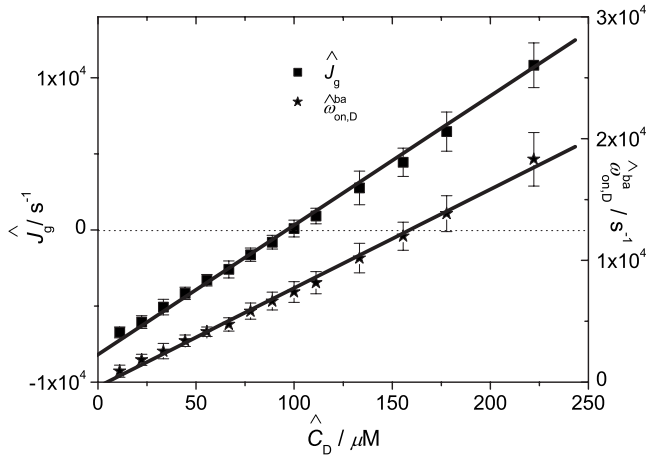


FIG. 6. Dependence of the ADP filament growth rate  $\hat{J}_g$  (left Y axis) and the inverse mean waiting time at the barbed end (right Y axis) on actin monomer concentrations  $\hat{C}_D$ . The intersection point of the square symbol curves with the horizontal dotted line defines the critical concentration  $\hat{C}_{D,\text{eq}}$ . The parameters are the same as in Fig. 3.

the bulk diffusion constant  $D$  and the capture zone volume, including the effect of binding free energy and changes in entropy.

### C. Binding times and attachment rates

The filament growth rate is determined by the frequency with which monomers bind to its ends. Figure 5(a) shows histograms of the time intervals or waiting times between successive monomer-binding events for the two ends of the filament. The waiting time for the next monomer-binding event to occur is expected to be stochastic and exponentially distributed. As shown in Fig. 5(a), the histogram is approximately exponential from which we can extract the mean waiting time  $\hat{\tau}_{\text{on},D}$  between monomer attachment events. In addition, the histograms are identical when the capture zone size is the same at both ends of the filament. The inverse mean waiting times as obtained from the exponential distribution are plotted in Fig. 5(b) as a function of the monomer concentration  $\hat{C}_D$  for different capture zones. It is clear that the inverse mean waiting time  $1/\hat{\tau}_{\text{on},D}$  increases linearly with the monomer concentration  $\hat{C}_D$ , i.e.,  $1/\hat{\tau}_{\text{on},D} \propto \hat{C}_D$ . Furthermore, the intercepts of these curves with the Y-axis at  $\hat{C}_D = 0$  are close to zero. Inspection of Fig. 5(b) also shows that  $1/\hat{\tau}_{\text{on},D}$  grows monotonically with the increasing capture zone size  $d$  for fixed concentration  $\hat{C}_D$ . Comparing Fig. 5(b) with Fig. 4, one finds that  $\hat{\omega}_{\text{on},D} = \hat{\kappa}_{\text{on},D} \hat{C}_D \approx 1/\hat{\tau}_{\text{on},D}$  as required for consistency. On the other hand, the mean waiting time  $\hat{\tau}_{\text{off},D}$  between two successive monomer-detachment events is equal to  $1/\hat{\omega}_{\text{off},D}$ . Thus, the growth rate of the ADP-actin filament in Eq. (24) can be expressed as

$$\begin{aligned} \hat{J}_g(\hat{C}_D) &= \frac{1}{\hat{\tau}_{\text{on},D}^{\text{ba}}} + \frac{1}{\hat{\tau}_{\text{on},D}^{\text{po}}} - \frac{1}{\hat{\tau}_{\text{off},D}^{\text{ba}}} - \frac{1}{\hat{\tau}_{\text{off},D}^{\text{po}}} \\ &= \hat{\omega}_{\text{on},D}^{\text{ba}} + \hat{\omega}_{\text{on},D}^{\text{po}} - \hat{\omega}_{\text{off},D}^{\text{ba}} - \hat{\omega}_{\text{off},D}^{\text{po}}. \end{aligned} \quad (25)$$

When the monomer concentration  $\hat{C}_D$  approaches  $\hat{C}_{D,\text{eq}}$ , the growth rate  $\hat{J}_g(\hat{C}_{D,\text{eq}}) \approx 0$  which implies  $(\hat{\tau}_{\text{on},D}^{\text{ba}})$

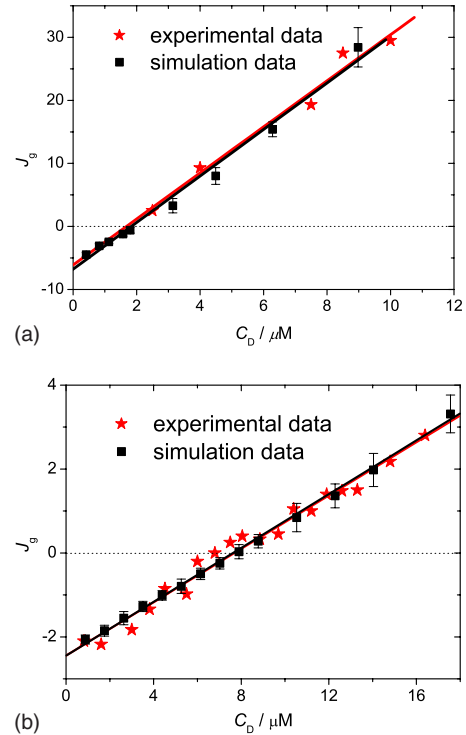


FIG. 7. The growth rate  $J_g$  as a function of  $C_D$ . (a) The experimental data and the simulation data in Fig. 6 are expressed in physical units with the rescaling factors  $b=1352$  and  $b_\kappa=27.3$ . (b) The experimental data are taken from Fig. 3 of Ref. 5 and the simulation data in Fig. 6 are expressed in physical units with the rescaling factors  $b=3265$  and  $b_\kappa=258$ . Note that the critical (or equilibrium) concentration at which the growth rate vanishes is rather different for the two sets of experimental data reflecting the different ionic conditions.

$+\hat{\tau}_{\text{on},D}^{\text{po}})/\hat{\tau}_{\text{on},D}^{\text{ba}}\hat{\tau}_{\text{on},D}^{\text{po}}=(\hat{\tau}_{\text{off},D}^{\text{ba}}+\hat{\tau}_{\text{off},D}^{\text{po}})/\hat{\tau}_{\text{off},D}^{\text{ba}}\hat{\tau}_{\text{off},D}^{\text{po}}$ . For general  $\hat{C}_D$ , the two ends of the filament perform biased random walks. The mean time interval for forward and backward steps at the barbed end are  $\hat{\tau}_{\text{on},D}^{\text{ba}}$  and  $\hat{\tau}_{\text{off},D}^{\text{ba}}$ , respectively, and likewise at the pointed end.

### D. Concentration dependence of growth rate

To provide insight into the behavior of the mean growth rate  $\hat{J}_g$  and the relation between growth rates and waiting times, Fig. 6 gives simulation results of the ADP filament's growth rate and the inverse mean waiting time at the barbed end as a function of free actin monomer concentration  $\hat{C}_D$ . As shown in Fig. 6, simple linear dependencies are found for both growth rate and the inverse of the mean waiting time as functions of  $\hat{C}_D$ , approximately obeying, respectively, Eq. (24) and the expression  $\hat{\omega}_{\text{on},D}^{\text{ba}}=1/\hat{\tau}_{\text{on},D}^{\text{ba}}=\hat{\kappa}_{\text{on},D}^{\text{ba}}\hat{C}_D$ . The slope and extrapolated value at  $\hat{C}_D=0$  are obtained from a least-squares fit of the data for the growth rate  $\hat{J}_g$  as a function of  $\hat{C}_D$ . This allows us to calculate the sum of the attachment rate constants and detachment rates at the barbed and pointed ends. We find that  $\hat{\kappa}_{\text{on},D}^{\text{ba}}+\hat{\kappa}_{\text{on},D}^{\text{po}}=84.9 \mu\text{M}^{-1} \text{s}^{-1}$  and  $\hat{\omega}_{\text{off},D}^{\text{ba}}+\hat{\omega}_{\text{off},D}^{\text{po}}=7.91 \times 10^3 \text{s}^{-1}$ . Thus, these simulated parameters are about 28-fold and 1400-fold larger than the experimental value given in Table I, respectively. It is also seen that the critical concentration  $\hat{C}_{D,\text{eq}}$  is close to  $93.2 \mu\text{M}$ , which is

about 50-fold larger than the value observed experimentally. Obviously, these parameters obtained from the simulation deviate slightly from the prescribed parameters, see Table II. Likewise, the curve of  $\hat{\omega}_{\text{on},D}^{\text{ba}}$  versus  $\hat{C}_D$  yields that the attachment rate constant  $\hat{\kappa}_{\text{on},D}^{\text{ba}}$  is equal to  $81 \mu\text{M}^{-1} \text{s}^{-1}$ , which is in good agreement with the above results. Using the rescaling factors,  $b$  and  $b_{\kappa}$ , the growth rate and monomer concentration can be expressed in physical units as presented in Fig. 7. Thus, the simulated dynamics of the ADP filaments is consistent with those observed in experiments.

## E. Length fluctuations and length diffusion constants

Finally, we analyze the fluctuations in the total filament length  $L=L(t)$  or in the total number  $n(t)=n^{\text{ba}}(t)+n^{\text{po}}(t)$  of added monomers as characterized by the corresponding variances

$$\begin{aligned} \langle [L - \langle L \rangle]^2 \rangle &= \langle [n - \langle n \rangle]^2 \rangle \\ &\approx \langle [n^{\text{ba}} - \langle n^{\text{ba}} \rangle]^2 \rangle + \langle [n^{\text{po}} - \langle n^{\text{po}} \rangle]^2 \rangle, \end{aligned} \quad (26)$$

where the asymptotic equality follows from the relation

$$\begin{aligned} \langle [n^{\text{ba}} - \langle n^{\text{ba}} \rangle][n^{\text{po}} - \langle n^{\text{po}} \rangle] \rangle \\ \approx \langle n^{\text{ba}} - \langle n^{\text{ba}} \rangle \rangle \langle n^{\text{po}} - \langle n^{\text{po}} \rangle \rangle = 0 \end{aligned} \quad (27)$$

for sufficiently long filaments. Note that all quantities that appear in the latter two equations depend, in general, on time  $t$ .<sup>27</sup>

The excess numbers  $n^{\text{ba}}$  and  $n^{\text{po}}$ , which are added to the barbed and point ends of the filament, undergo biased random walks. Thus, let us briefly review the statistical properties of a random walk in continuous time  $t$  that moves on the discrete state space of integers denoted by  $m$ . The walker steps forward with rate  $\omega_{\text{on}}$  and backward with rate  $\omega_{\text{off}}$ . The time-dependent probability  $P_m = P_m(t)$ , to find the walker in state  $m$ , then satisfies the master equation

$$\frac{\partial}{\partial t} P_m = P_{m-1} \omega_{\text{on}} + P_{m+1} \omega_{\text{off}} - P_m (\omega_{\text{on}} + \omega_{\text{off}}) \quad (28)$$

with the initial condition

$$P_m(t=0) = \delta(m,0), \quad (29)$$

where  $\delta(m,0)=1$  for  $m=0$  and  $\delta(m,0)=0$  otherwise. The moments of the probability distribution  $P_m(t)$  can be obtained from the auxiliary function

$$Q(z,t) \equiv \sum_{m=-\infty}^{+\infty} z^m P_m(t) \quad (30)$$

and the quantities

$$Q_k(t) \equiv \left. \frac{\partial^k}{\partial z^k} Q(z,t) \right|_{z=1}. \quad (31)$$

The mean value  $\langle m(t) \rangle$  and the variance  $\langle [m(t) - \langle m(t) \rangle]^2 \rangle$ , for example, are given by the identities

$$\begin{aligned} \langle m(t) \rangle &= Q_1(t) \quad \text{and} \quad \langle [m(t) - \langle m(t) \rangle]^2 \rangle = Q_2 + Q_1 - Q_1^2. \end{aligned} \quad (32)$$

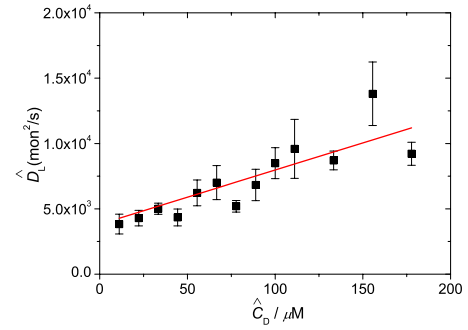


FIG. 8. Length diffusion constant  $\hat{D}_L$  (solid squares) as defined in Eq. (39) for ADP-actin polymerization. The solid (red) line represents the analytical expression (41). The parameters are the same as in Fig. 3.

For the master Eq. (28) with the initial condition (29), the auxiliary function  $Q(z,t)$  can be calculated explicitly by multiplying the master equation with  $z^m$  and summing both sides of this equation over all  $m$ . One then obtains a differential equation for  $Q(z,t)$  with the initial condition  $Q(z,0) = 1$ , which leads to the explicit solution

$$Q(z,t) = e^{g(z)t} \quad \text{with} \quad g(z) \equiv \omega_{\text{on}}z + \omega_{\text{off}}z^{-1} - (\omega_{\text{on}} + \omega_{\text{off}}). \quad (33)$$

Inserting this expression for  $Q(z,t)$  into relation (32), we obtain the mean value

$$\langle m(t) \rangle = (\omega_{\text{on}} - \omega_{\text{off}})t \quad (34)$$

and the variance

$$\langle [m(t) - \langle m(t) \rangle]^2 \rangle = (\omega_{\text{on}} + \omega_{\text{off}})t. \quad (35)$$

We now use the expressions (34) and (35) for the two numbers  $m=n^{(\alpha)}$  with  $\alpha=\text{ba}$  and  $\alpha=\text{po}$  that are added at the barbed and pointed filament ends, respectively. When we use the expression (34) for the mean value  $\langle m(t) \rangle$ , we recover the relation (23) for the average growth rate of the filament. In addition, the expression (35) for the variance  $\langle [m(t) - \langle m(t) \rangle]^2 \rangle$  implies that

$$\langle [n^{(\alpha)} - \langle n^{(\alpha)} \rangle]^2 \rangle \approx 2D_L^{(\alpha)}t = 2\hat{D}_L^{(\alpha)}\hat{t} \quad (36)$$

for large  $t$  or  $\hat{t}$  with the diffusion constants

$$D_L^{(\alpha)} = \frac{1}{2}(\omega_{\text{on}}^{(\alpha)} + \omega_{\text{off}}^{(\alpha)})\text{mon}^2 \quad (37)$$

or

$$\hat{D}_L^{(\alpha)} = \frac{1}{2}(\hat{\omega}_{\text{on}}^{(\alpha)} + \hat{\omega}_{\text{off}}^{(\alpha)})\text{mon}^2 = bD_L^{(\alpha)}, \quad (38)$$

where “mon” is an abbreviation for “monomer.”

A combination of the relations (36) and (26) now implies that the variance of the filament length fluctuations behaves as

$$\langle [L - \langle L \rangle]^2 \rangle \approx 2D_L t = 2\hat{D}_L \hat{t} \quad (39)$$

for large  $t$  or  $\hat{t}$  with the relations

$$D_L \equiv D_L^{\text{ba}} + D_L^{\text{po}} = \hat{D}_L/b \quad (40)$$

and the diffusion constant

$$D_L = \frac{1}{2}(\omega_{\text{on}}^{\text{ba}} + \omega_{\text{off}}^{\text{ba}} + \omega_{\text{on}}^{\text{po}} + \omega_{\text{off}}^{\text{po}})\text{mon}^2$$

$$= \frac{1}{2}[\omega_{\text{off}}^{\text{ba}} + \omega_{\text{off}}^{\text{po}} + (\kappa_{\text{on}}^{\text{ba}} + \kappa_{\text{on}}^{\text{po}})C_D]\text{mon}^2. \quad (41)$$

In Fig. 8, we compare the analytical expression (41) with numerical results for the diffusion constant  $\hat{D}_L = bD_L$ . For small concentrations of ADP-actin corresponding to continuous depolymerization of the filament, the length diffusion constant attains the constant value

$$D_L \approx \frac{1}{2}(\omega_{\text{off}}^{\text{ba}} + \omega_{\text{off}}^{\text{po}})\text{mon}^2 \text{ for small } C_D. \quad (42)$$

For the equilibrium (or critical) concentration  $C_D = C_{D,\text{eq}}$ , the attachment and detachment rates are equal at each end, and we obtain

$$D_L = (\omega_{\text{off},D}^{\text{ba}} + \omega_{\text{off},D}^{\text{po}})\text{mon}^2 \text{ for } C_D = C_{D,\text{eq}}. \quad (43)$$

Using the numerical values in Table I or Table II, one obtains  $D_L = 5.65 \text{ mon}^2/\text{s}$  or  $\hat{D}_L = 7.64 \times 10^3 \text{ mon}^2/\text{s}$  for the equilibrium (or critical) concentration  $C_D = C_{D,\text{eq}}$ . For increasing concentration  $C_D$  of ADP-actin, the length diffusion constant grows linearly with  $C_D$  as in Eq. (41).

#### IV. CONCLUSIONS AND OUTLOOK

We have used BD simulations to study the dynamical processes that govern the self-assembly or polymerization of ADP-actin. In order to study the dynamics of long filaments consisting of up to several hundred protomers, we used a coarse-grained model for actin polymerization, which involves several simplifications as well as an overall rescaling of time. First, we ignored the atomic details of the actin monomers and described them as in Fig. 1(a). Second, free monomers were taken to interact via soft-core potentials as given by Eq. (3), a form that has been widely used in dissipative particle dynamics. Third, we did not simulate the initial nucleation process, which requires three monomers to bind simultaneously and which would typically take a relatively long time. Instead, each filament was seeded at the beginning of the simulation with only two monomers that were labeled as its barbed and pointed ends, respectively. Our simulations are performed at constant concentration of freely diffusing actin monomers. This is achieved by adding a monomer at a randomly chosen position far away from the filament when a monomer has attached to this filament and by removing the newly detached monomers.<sup>25</sup>

In order to overcome the large separation of time scales between the diffusive motion of the free monomers and the relatively slow attachment and detachment processes at the two ends of the filaments, we rescaled all attachment and detachment rates by the same factor  $b$ , see the relations in Eqs. (13)–(19). In this way, we speed up all dynamical processes related to actin polymerization and depolymerization by the same factor  $b$ . If the rescaling factor  $b$  is chosen to be of the order of  $10^3$ , the polymerization dynamics of long actin filaments consisting of hundreds of protomers becomes accessible to BD simulations. In the simulations reported here, we chose  $b = 1352$  and used this factor to transform the experimentally measured rates in Table I into the rescaled rates in Table II.

Our rescaling procedure has been defined in such a way that (i) the ratio of the rescaled attachment rate constants  $\hat{\kappa}_{\text{on}}$  is equal to the ratio of the measured attachment rate constants  $\kappa_{\text{on}}$ , see Eqs. (16) and (17), and that (ii) the size of the capture zones at the two filament ends is comparable to the size of a free actin monomer. These two requirements imply that we increase the monomer concentration by a certain rescaling factor as in Eq. (19). As far as filament polymerization and depolymerization are concerned, the real system at time  $t$  then corresponds to the simulated system at time  $\hat{t} = t/b$ . The only drawback of our rescaling procedure is that the diffusive motion of the actin monomers is now too slow compared to the attachment and detachment processes. Thus, if we did not remove the newly detached monomers, these monomers would reattach too frequently.

In order to demonstrate the feasibility of our approach, we have focused on the simplest situation, which is provided by the self-assembly of ADP-actin as studied experimentally in Refs. 5–9. This case is used to unravel certain relations between the filament's physical properties and the model parameters such as between the attachment rate constant and the size of the capture zone, see Fig. 4, or between the growth rate and the waiting times for two successive attachment/detachment events, see Fig. 5. When a single filament grows in a bath of constant concentration of free ADP-actin monomers, its growth rate increases linearly with the free monomer concentration and agrees quantitatively with the *in vitro* experiments in Refs. 5 and 7, as shown in Figs. 7(a) and 7(b), respectively. We also studied the fluctuations in the filament length and found that the corresponding diffusion constant attains the constant value (42) at small ADP-actin concentrations  $C_D$  and grows linearly with increasing  $C_D$  as in Eq. (41), compare Fig. 8.

Our approach can now be extended to the self-assembly and polymerization of ATP-actin for which the actin protomer within the filament can attain three different states corresponding to ATP-actin, ADP/P-actin, and ADP-actin. Preliminary studies show that such simulations can be used to demonstrate the process of treadmilling and to study the coupling between polymerization and ATP hydrolysis. Likewise, our approach can be used to address more complex processes involving filament bundles and externally applied forces, which should then provide additional insight into the corresponding biological processes.

#### ACKNOWLEDGMENTS

We thank Xin Li for the stimulating discussions and acknowledge support by Grant No. RGP0072 of the Human Frontier Science Project. MEMPHYS is supported by the Danish National Research Foundation.

#### APPENDIX: IMPLEMENTATION OF CHEMICAL EQUILIBRIUM

In order to implement chemical equilibrium at both ends of the filament, we need to ensure that the equilibrium (or critical) concentration  $C_{D,\text{eq}}$  has (essentially) the same value at both ends. This is done as follows. First, the filament is capped at the pointed end so that the filament grows only at

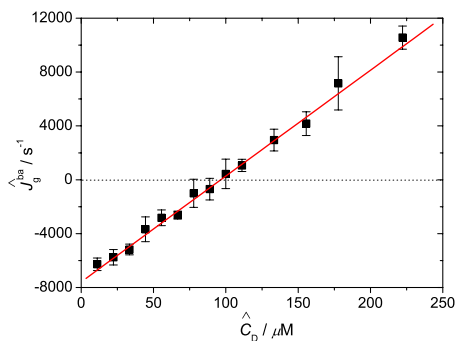


FIG. 9. The growth rate  $\hat{J}_g^{\text{ba}}$  (solid squares) as a function of  $\hat{C}_D$ . The solid (red) line is a linear fit. The detachment rate  $\hat{\omega}_{\text{off},D}^{\text{ba}}=7.3 \times 10^3 \text{ s}^{-1}$  and the capture zone size  $d^{\text{ba}}=2.5r_0$ .

the barbed end. We choose the capture zone size  $d^{\text{ba}}=2.5r_0$  and the detachment rate  $\hat{\omega}_{\text{off},D}^{\text{ba}}=7.3 \times 10^3 \text{ s}^{-1}$ . The growth rate  $\hat{J}_g^{\text{ba}}$  at the barbed end of the filament is presented in Fig. 9 as a function of actin monomer concentrations  $\hat{C}_D$  with these simulation parameters. These data imply that the critical concentration at the barbed end is  $\hat{C}_{D,\text{eq}}^{\text{ba}}=92.04 \pm 2.56 \text{ }\mu\text{M}$  and the attachment rate constant  $\hat{\kappa}_{\text{on},D}^{\text{ba}}=\hat{\omega}_{\text{off},D}^{\text{ba}}/\hat{C}_{D,\text{eq}}^{\text{ba}}$  is  $79.31 \pm 2.28 \text{ }\mu\text{M}^{-1} \text{ s}^{-1}$ . Next, the barbed

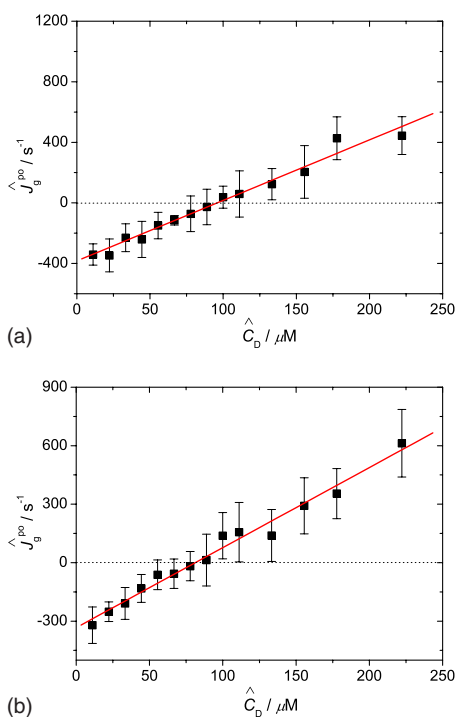


FIG. 10. The growth rate  $\hat{J}_g^{\text{po}}$  (solid squares) as a function of  $\hat{C}_D$ ,  $\hat{\omega}_{\text{off},D}^{\text{po}}=338 \text{ s}^{-1}$ . The solid (red) line is a linear fit. (a) The capture zone size  $d^{\text{po}}=0.84r_0$ . (b) The capture zone size  $d^{\text{po}}=0.85r_0$ .

end is capped so that the filament grows only at the pointed end. For  $X_\kappa=21.6$ , we choose the detachment rate  $\hat{\omega}_{\text{off},D}^{\text{po}}=338 \text{ s}^{-1}$  and the capture zone size  $d^{\text{po}}$  to be  $0.84r_0$  and  $0.85r_0$ . In Figs. 10(a) and 10(b), we plot the corresponding data for the growth rate  $\hat{J}_g^{\text{po}}$  at the pointed end as a function of ADP concentration  $\hat{C}_D$ . The inspection of these two figures shows that  $\hat{C}_{D,\text{eq}}^{\text{po}}=94.32 \pm 5.72 \text{ }\mu\text{M}$  for  $d^{\text{po}}=0.84r_0$  and  $\hat{C}_{D,\text{eq}}^{\text{po}}=77.23 \pm 9.82 \text{ }\mu\text{M}$  for  $d^{\text{po}}=0.85r_0$ . The linear interpolation between these two values then implies that the choice  $d^{\text{po}}=0.8413r_0$  leads to the critical concentration  $\hat{C}_{D,\text{eq}}^{\text{po}}=92.04 \pm 3 \text{ }\mu\text{M}$ , i.e., to the same value as determined previously for the barbed end. In addition, the attachment rate constant  $\hat{\kappa}_{\text{on},D}^{\text{po}}$  is found to be  $3.67 \pm 0.083 \text{ }\mu\text{M}^{-1} \text{ s}^{-1}$ .

<sup>1</sup>B. Lodish and K. Matsudaira, *Molecular Cell Biology*, 5th ed. (Freeman, San Francisco, 2003).

<sup>2</sup>A. Wegner, *J. Mol. Biol.* **108**, 139 (1976).

<sup>3</sup>M. F. Carlier and D. Pantaloni, *J. Biol. Chem.* **282**, 23005 (2007).

<sup>4</sup>T. D. Pollard, *Annu. Rev. Biophys. Biomol. Struct.* **36**, 451 (2007).

<sup>5</sup>M. F. Carlier, D. Pantaloni, and E. D. Korn, *J. Biol. Chem.* **259**, 9983 (1984).

<sup>6</sup>T. D. Pollard, *J. Cell Biol.* **99**, 769 (1984).

<sup>7</sup>T. D. Pollard, *J. Cell Biol.* **103**, 2747 (1986).

<sup>8</sup>T. Ohm and A. Wegner, *Biochim. Biophys. Acta* **1208**, 8 (1987).

<sup>9</sup>E. D. Korn, M. F. Carlier, and D. Pantaloni, *Science* **238**, 638 (1987).

<sup>10</sup>L. Blanchoin and T. D. Pollard, *Biochemistry* **41**, 597 (2002).

<sup>11</sup>M. F. Carlier and D. Pantaloni, *Biochemistry* **25**, 7789 (1986).

<sup>12</sup>I. Fujiwara, D. Vavylonis, and T. D. Pollard, *Proc. Natl. Acad. Sci. U.S.A.* **104**, 8827 (2007).

<sup>13</sup>D. Vavylonis, Q. B. Yang, and B. O. Shaughnessy, *Proc. Natl. Acad. Sci. U.S.A.* **102**, 8543 (2005).

<sup>14</sup>T. D. Pollard and A. G. Weeds, *FEBS Lett.* **170**, 94 (1984).

<sup>15</sup>D. Pantaloni, M. F. Carlier, and E. D. Korn, *J. Biol. Chem.* **260**, 6572 (1985).

<sup>16</sup>E. B. Stukalin and A. B. Kolomeisky, *Biophys. J.* **90**, 2673 (2006).

<sup>17</sup>D. Sept and J. A. McCammon, *Biophys. J.* **81**, 667 (2001).

<sup>18</sup>I. Fujiwara, S. Takahashi, H. Tadakuma, T. Funatsu, and S. Ishiwata, *Nat. Cell Biol.* **4**, 666 (2002).

<sup>19</sup>M. P. Allen and D. J. Tildesley, *Computer Simulation of Liquids* (Oxford Science Publications, Oxford, 1987).

<sup>20</sup>D. L. Ermak and J. A. McCammon, *J. Chem. Phys.* **69**, 1352 (1978).

<sup>21</sup>D. Sept, A. H. Elcock, and J. A. McCammon, *J. Mol. Biol.* **294**, 1181 (1999).

<sup>22</sup>J. C. Shillcock and R. Lipowsky, *J. Chem. Phys.* **117**, 5048 (2002).

<sup>23</sup>J. A. Cooper, S. B. Walker, and T. D. Pollard, *J. Muscle Res. Cell Motil.* **4**, 253 (1983).

<sup>24</sup>N. G. Van Kampen, *Stochastic Processes in Physics and Chemistry*, 3rd ed. (Elsevier, New York, 1992).

<sup>25</sup>As explained in Sec. II D, we speed up all attachment and detachment processes by the same factor  $b$ . This implies that the diffusion of the detached monomer out of the capture zone is now too slow compared to the reattachment of this monomer to the filament end. The removal of the detached monomer has the additional advantage that it avoids this artificial increase in the reattachment rate.

<sup>26</sup>J. L. McGrath and Y. Tardy, *Biophys. J.* **75**, 2070 (1998).

<sup>27</sup>Strictly speaking, the ensemble of filaments that defines the averages in Eqs. (26) and (27) consists of the subset of filaments that has not disappeared by depolymerization up to time  $t$ .